

A current density conservative scheme for incompressible MHD flows at a low magnetic Reynolds number. Part II: On an arbitrary collocated mesh

Ming-Jiu Ni ^{a,c,*}, Ramakanth Munipalli ^b, Peter Huang ^b, Neil B. Morley ^a,
Mohamed A. Abdou ^a

^a MAE Department, University of California at Los Angeles, CA 90095, USA

^b HyperComp Inc., Westlake Village, CA 91362, USA

^c Physics Department, Graduate University of Chinese Academy of Sciences, Beijing 100049, China

Received 19 October 2006; received in revised form 16 April 2007; accepted 22 July 2007

Available online 8 August 2007

Abstract

A conservative formulation of the Lorentz force is given here for magnetohydrodynamic (MHD) flows at a low magnetic Reynolds number with the current density calculated based on Ohm's law and the electrical potential formula. This conservative formula shows that the total momentum contributed from the Lorentz force is conservative when the applied magnetic field is constant. For the case with a non-constant applied magnetic field, the Lorentz force has been divided into two parts: a strong globally conservative part and a weak locally conservative part.

The conservative formula has been employed to develop a conservative scheme for the calculation of the Lorentz force on an unstructured collocated mesh. Only the current density fluxes on the cell faces, which are calculated using a consistent scheme with good conservation, are needed for the calculation of the Lorentz force. Meanwhile, a conservative interpolation technique is designed to get the current density at the cell center from the current density fluxes on the cell faces. This conservative interpolation can keep the current density at the cell center conservative, which can be used to calculate the Lorentz force at the cell center with good accuracy. The Lorentz force calculated from the conservative current at the cell center is equivalent to the Lorentz force from the conservative formula when the applied magnetic field is constant, which can conserve the total momentum. We will further prove that the simple interpolation scheme used in the Part I [M.-J. Ni, R. Munipalli, N.B. Morley, P.Y. Huang, M. Abdou, A current density conservative scheme for MHD flows at a low magnetic Reynolds number. Part I. On a rectangular collocated grid system, *Journal of Computational Physics*, in press, doi:10.1016/j.jcp.2007.07.025] of this series of papers is conservative on a rectangular grid and can keep the total momentum conservative in a rectangular grid.

© 2007 Elsevier Inc. All rights reserved.

Keywords: Conservative formula of the Lorentz force; Consistent and conservative scheme; Projection method; MHD

* Corresponding author. Address: Physics Department, Graduate University of Chinese Academy of Sciences, Beijing 100049, China.
E-mail addresses: mjni@gucas.ac.cn, mjni@ucla.edu (M.-J. Ni).
URL: <http://www.fusion.ucla.edu> (M.A. Abdou).

1. Introduction

Magnetohydrodynamic (MHD) flows of electrically conducting liquids at high Hartmann numbers has been a topic of great interest in the development of a fusion reactor blanket [1–4]. Two-dimensional MHD flows in a channel have been extensively studied by theoretical analysis and numerical simulation [5–8]. The Hartmann number Ha is a measure of the magnetic field strength for a given fluid in a duct of a given scale. The thickness of the Hartmann layers on all walls normal to field scales with Ha^{-1} and is very thin; the side layers on all walls parallel to the magnetic field scale with $Ha^{-1/2}$ and are much thicker than the Hartmann layers at high Hartmann numbers. The development of fusion reactors experiments with strong magnetic fields leads to a growing interest in the study of 3D MHD phenomena. When inertial terms are small, the asymptotic method [9–11] that focuses on the main phenomena is a very efficient method to compute 3D MHD flows. This efficient method is valid for high Hartmann numbers and high interaction parameters, but cannot always handle arbitrary complex geometries. When inertial terms are important, the direct simulation method accounting for all the physical effects is an important tool to study the 3D MHD phenomena. Using the direct simulation method, a very fine mesh is required to resolve the Hartmann layer and the side layer at high Hartmann numbers. For unsteady flows, the time step is proportional to the smallest grid size with an explicit update of the temporal term. The cost of direct simulation of 3D MHD flows at high Hartmann number is high since it requires a fine mesh and therefore a small time step for unsteady flows. Three-dimensional numerical simulations of inertial flows are often limited to the steady regime and low Hartmann numbers.

For low magnetic Reynolds numbers, the electrical potential formula can be employed for MHD with good accuracy [12,13]. Consider the fully developed MHD flow in a rectangular channel, where flow velocity is in the x -direction and magnetic field is applied in the y -direction. All derivatives with respect to x are zero except for that of pressure, which is a constant in the flow and zero in solid wall regions. Current is computed from Ohm's law as

$$\mathbf{J} = (0, j_y, j_z) = \sigma \left(0, -\frac{\partial \varphi}{\partial y}, -\frac{\partial \varphi}{\partial z} + u \right). \quad (1)$$

In the core of the flow away from any viscous or inertial boundary layers, the Lorentz force is balanced by the pressure gradient, as illustrated in [14], which leads to the following relations:

$$\frac{dp}{dx} = \frac{Ha^2}{Re} \left(-\frac{\partial \varphi}{\partial z} + u \right) \quad (2)$$

At high Ha with a given pressure gradient which corresponds to a given flow rate, the right hand side of the above equation is very small. The core dimensionless velocity being close to 1 requires the dimensionless gradient of the electric potential above to be also close to 1 in magnitude, but opposite in sign. We then have a situation in which current is computed from the difference between two large and nearly identical numbers. It turns out that this imposes some restrictions on the manner in which current is numerically computed from the electric potential. An elaborate algorithm is needed for the calculation of MHD at high Hartmann numbers.

For incompressible MHD flow, a staggered grid system [15], a fully staggered grid system [16–18] and a collocated grid system [19,20,14] have been employed to do the direct simulations. The staggered grid system can effectively avoid the checkerboard phenomenon of pressure. However, it is hard to construct a current density conservative scheme on a non-uniform staggered grid system. A fully staggered grid system can be employed to conserve the current density with a uni-directional applied magnetic field [16]. However, it is hard to extend the conservative scheme to a case with multi-directional applied magnetic field. Also it is not easy to construct a current density conservative scheme on an unstructured staggered and fully staggered grid systems.

Ni et al. [14] developed a current density conservative scheme on a rectangular collocated mesh, as shown in Fig. 1(a). In this collocated grid, velocity (\mathbf{u}), pressure (p), and electrical potential (φ) are located in the grid center, while current fluxes are located on the cell faces. A consistent scheme is presented to get the divergence-free current fluxes on the cell faces of a control volume. A simple conservative interpolation technique is

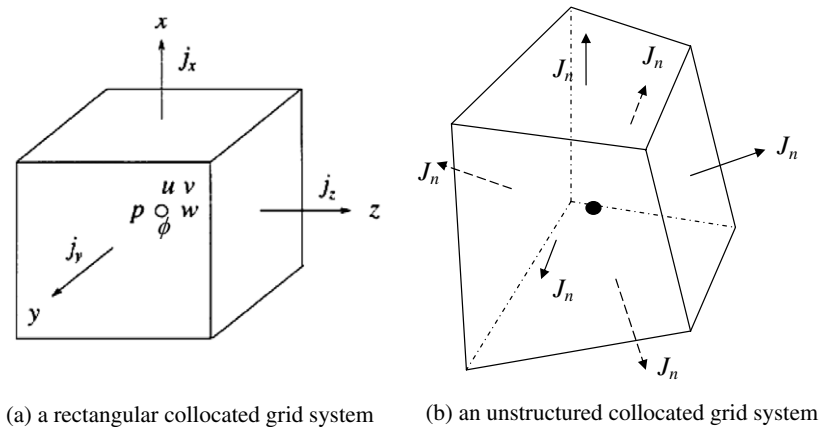


Fig. 1. Collocated grid arrangement.

designed on a rectangular collocated grid to get the current density at the cell center by interpolating the divergence-free current fluxes on the cell faces. This current density conservative scheme can keep the current density at the cell center conservative, which is used to calculate the Lorentz force. Numerical validations have been given in [14] to show that the current density conservative scheme has a good resolution at the side layers and the Hartmann layers, even at high Hartmann numbers.

In the momentum equations, the Lorentz force exists as a source term in an explicit non-conservative form. We have noted that the Lorentz force in the momentum equations has a similar form as the Coriolis force has on a rotating coordinate system. The disadvantages of this non-conservative form of the Coriolis force on a rotating frame were reported in [21], which indicated that the explicit treatment of the Coriolis force may lead to erroneous results in a rotating frame. Agarwal and Deese [22] have absorbed half of the Coriolis force into the divergence form. Based on this divergence form of the Coriolis force, Beddhu et al. [23] have successfully formulated the Navier–Stokes equations in a fully conservative form without the traditional source terms in the case of a rotating reference frame. Using a similar idea as used in Agarwal and Deese [22], we will cast the Lorentz force in the globally and locally conservative forms. The formulation is equivalent to the original non-conservative form from a theoretical point of view, but there exist differences between these formulations from a numerical point of view. In this paper, we will show how the conservative form of the Lorentz force can help us construct a consistent and conservative scheme for the calculation of the Lorentz force. Based on this conservative formulation of the Lorentz force, a conservative interpolation technique is developed to calculate the current density at the cell center from the current fluxes on the cell faces of a control volume. We will further prove that the simple interpolation technique in [14] is conservative in a rectangular coordinate, which can conserve the total momentum when the applied magnetic field is constant.

The general second-order temporal accuracy projection method [14] developed for MHD flows will be further extended on a collocated unstructured mesh (Fig. 1(b)) with the Lorentz force included as a source term in the Navier–Stokes equations. This projection method can accurately and effectively balance the pressure term and Lorentz force at the fully developed core flow as shown in [14]. This projection method can also simplify the pressure boundary conditions for the Navier–Stokes equations with the Lorentz force considered. Since it has been proven that the SIMPLE-type methods are special cases of this general projection method, the existed research and commercial codes based on the SIMPLE type methods, such as the commercial codes of CFX [24], FLUENT [25] and SC/TETRA [26], can be used to conduct the calculation of MHD flows using the technique developed in this paper and our previous paper [14] by solving the electrical potential equation for low magnetic Reynolds numbers.

In this paper, a conservative formulation of the Lorentz force is developed in Section 2. The current density and Lorentz force conservative schemes on an unstructured mesh have been developed in Section 3. Section 4 gives the detailed computational procedures for the simulation of MHD flows on an arbitrary unstructured mesh based on the general second-order projection method. Several numerical simulations are conducted

to validate that the consistent and conservative schemes can be employed for high Hartmann MHD flows on an arbitrary unstructured mesh in Section 5. Section 6 summarizes the contributions of this paper. In Appendix A, Hunt's and Shercliff's analytical formulas have been reformulated for accurate computations without further approximation at high Hartmann numbers.

2. Conservative formula of the Lorentz force

The flow of electrically conducting fluid under the influence of an external magnetic field is governed by the following Navier–Stokes equation and continuity equation, which represent the conservation of momentum and mass:

$$\frac{\partial \mathbf{u}}{\partial t} + \mathbf{u} \cdot \nabla \mathbf{u} = -\nabla p + \frac{1}{Re} \nabla^2 \mathbf{u} + N(\mathbf{J} \times \mathbf{B}) \quad (3)$$

$$\nabla \cdot \mathbf{u} = 0 \quad (4)$$

where \mathbf{u} , p are the non-dimensional velocity vector and kinetic pressure scaled with v_0 and ρv_0^2 respectively. With L defined as characteristic length, $Re = v_0 L / \eta$ is the Reynolds number, $Ha = LB_0 \sqrt{\sigma / \rho \eta}$ is the Hartmann number, and $N = Ha^2 / Re$ is the interaction parameter. \mathbf{J} represents the current density, and \mathbf{B} is the applied magnetic field scaled with $\sigma v_0 B_0$ and B_0 respectively. Also we define the magnetic Reynolds number here as $Re_m = \mu \sigma L v_0$, where η and σ are the fluid viscosity and conductivity respectively. μ is the permeability of the fluid and the walls, ρ is the density of the fluid. The term $N(\mathbf{J} \times \mathbf{B})$ is the Lorentz force, which is a volume force in a non-conservative form in the momentum equation (3).

For a low magnetic Reynolds number, the flow of electrically conducting fluid under the influence of an external magnetic field with negligible induced field, the current density can be calculated through Ohm's law [12,13]

$$\mathbf{J} = -\nabla \varphi + \mathbf{u} \times \mathbf{B} \quad (5)$$

The current density is conservative, such that

$$\nabla \cdot \mathbf{J} = 0 \quad (6)$$

From Eqs. (5) and (6), we can get the electrical potential Poisson equation as

$$\nabla \cdot (\nabla \varphi) = \nabla \cdot (\mathbf{u} \times \mathbf{B}) \quad (7)$$

In a non-inertial rotating reference frame, the Coriolis and centrifugal acceleration terms are produced as source terms in the Navier–Stokes equation, which is not in the conservative form. The explicit treatment of the Coriolis force has been reported to lead to erroneous results in a rotating coordinate system [21]. Agarwal and Deese [22] cast the Coriolis force in the divergence form by noting the following formula:

$$\boldsymbol{\omega} \times \mathbf{u} = \mathbf{u} \cdot \nabla (\boldsymbol{\omega} \times \mathbf{r}) \quad (8)$$

Here, $\boldsymbol{\omega}$ is the rotating speed vector of the reference frame relative to the absolute inertial frame, \mathbf{r} is the distance vector. Similarly, when the applied magnetic field is constant, we have a corresponding formula for the Lorentz force as

$$\mathbf{B} \times \mathbf{J} = \mathbf{J} \cdot \nabla (\mathbf{B} \times \mathbf{r}) \quad (9)$$

Furthermore, when the applied magnetic field is not constant, we can get the following equivalent formulation of the Lorentz force:

$$\mathbf{J} \times \mathbf{B} = -\mathbf{J} \cdot \nabla (\mathbf{B} \times \mathbf{r}) + (\mathbf{J} \cdot \nabla \mathbf{B}) \times \mathbf{r} \quad (10)$$

Since the current density is conservative, Eq. (10) can be expressed as a divergence form based on Eq. (6) as

$$\mathbf{J} \times \mathbf{B} = -\nabla \cdot (\mathbf{J}(\mathbf{B} \times \mathbf{r})) + \nabla \cdot (\mathbf{J}\mathbf{B}) \times \mathbf{r} \quad (11)$$

When the applied magnetic field is constant or spatial coordinate independent, we get a strong conservative formula of the Lorentz force as

$$\mathbf{J} \times \mathbf{B} = -\nabla \cdot (\mathbf{J}(\mathbf{B} \times \mathbf{r})) \tag{12}$$

Therefore, the Lorentz force in Eq. (11) has been cast into two terms: a globally conservative term of $-\nabla \cdot (\mathbf{J}(\mathbf{B} \times \mathbf{r}))$ and a locally conservative term of $\nabla \cdot (\mathbf{J}\mathbf{B}) \times \mathbf{r}$. With the applied magnetic field known, it will be convenient to employ Eq. (11) for the calculation of the Lorentz force without any interpolation of current density from the cell faces to the cell center of a controlled volume in a cell-centered collocated mesh. We, then, have the following momentum equation as:

$$\frac{\partial \mathbf{u}}{\partial t} + \nabla \cdot (\mathbf{u}\mathbf{u} + N\mathbf{J}(\mathbf{B} \times \mathbf{r})) = -\nabla p + \frac{1}{Re} \nabla \cdot \nabla \mathbf{u} + N\nabla \cdot (\mathbf{J}\mathbf{B}) \times \mathbf{r} \tag{13}$$

The momentum equation of Eq. (13) can be reduced to the following strong conservative form when the applied magnetic field is constant

$$\frac{\partial \mathbf{u}}{\partial t} + \nabla \cdot \left(\mathbf{u}\mathbf{u} + N\mathbf{J}(\mathbf{B} \times \mathbf{r}) + p\mathbf{I} - \frac{1}{Re} \nabla \mathbf{u} \right) = 0 \tag{14}$$

The integral formula of Eq. (14) can be given as

$$\int_{\Omega} \frac{\partial \mathbf{u}}{\partial t} d\Omega + \oint_S \mathbf{n} \cdot \left(\mathbf{u}\mathbf{u} + N\mathbf{J}(\mathbf{B} \times \mathbf{r}) + p\mathbf{I} - \frac{1}{Re} \nabla \mathbf{u} \right) ds = 0 \tag{15}$$

Furthermore, the integral formula of the Lorentz force can be given as

$$\int_{\Omega} \nabla \cdot (\mathbf{J}(\mathbf{B} \times \mathbf{r})) d\Omega = \oint_S \mathbf{n} \cdot (\mathbf{J}(\mathbf{B} \times \mathbf{r})) ds = \oint_S J_n(\mathbf{B} \times \mathbf{r}) ds \tag{16}$$

which is only dependent on the boundary conditions of the flow region and clearly shows that the contribution on the total momentum from the Lorentz force is null for insulated walls, although the work conducted by the Lorentz force is non-zero [12]. The work due to the Lorentz force is

$$(\mathbf{J} \times \mathbf{B}) \cdot \mathbf{u} = -(\mathbf{u} \times \mathbf{B}) \cdot \mathbf{J} = -\mathbf{J}^2 - \nabla \cdot (\varphi \mathbf{J}) \tag{17}$$

The conservation of the total momentum from the Lorentz force (Eq. (16)) is a very important property. We believe that only the numerical schemes, which can numerically conserve the total momentum when the applied magnetic field is constant, can get an accurate result for MHD flows. We will prove later that the current density conservative scheme developed in [14] can conserve the total momentum at a rectangular grid, while the non-conservative schemes listed in [14] cannot.

3. Consistent and conservative schemes

In this section, a consistent and conservative scheme is developed on an arbitrary collocated unstructured mesh to calculate the current flux on a cell face, and the Lorentz force at the cell center. In Section 3.1, a consistent scheme is developed to calculate the current fluxes on cell faces of a controlled volume, which can ensure the current density is divergence-free in the controlled volume. In Section 3.2, two schemes are developed to conservatively calculate the Lorentz force, one is based on the conservative formulation of the force, and the other one is based on a conservative current density interpolated from the current fluxes. In Section 3.3, for the sake of comparison, an inconsistent and non-conservative scheme is given for the calculation of the Lorentz force.

3.1. Consistent scheme for calculation of current flux on cell face

Integrating Eq. (6) on a controlled volume of an unstructured mesh, as shown in Fig. 1(b), we have

$$\int_{\Omega} \nabla \cdot \mathbf{J} d\Omega = \oint_S \mathbf{n} \cdot \mathbf{J} ds = \sum_{f=1}^{nf} (\mathbf{n} \cdot \mathbf{J})_f s_f \tag{18}$$

Subscript f denotes a cell face, \mathbf{n}_f and s_f denote the outward normal direction and the area of a cell face respectively. nf is the number of cell faces of a controlled volume with $nf = 6$ for a hexahedral mesh, $nf = 4$ for a tetrahedral mesh, and $nf = 5$ for a prism mesh. It is a natural way to put the current density fluxes on the cell faces, as shown in Fig. 1(b), which can effectively conserve the current density in a controlled volume. From Eq. (5) of the Ohm's law, the current flux on a cell face can be calculated using

$$(J_n)_f = (\mathbf{J} \cdot \mathbf{n})_f = -(\nabla\varphi \cdot \mathbf{n})_f + \mathbf{n}_f \cdot (\mathbf{u} \times \mathbf{B})_f \tag{19}$$

As we have emphasized in [14], a consistent scheme is needed to conduct the calculation of $(\nabla\varphi)_f \cdot \mathbf{n}_f$, the gradient of the electrical potential, and the $(\mathbf{u} \times \mathbf{B})_f \cdot \mathbf{n}_f$ on the cell faces, which can ensure that the current density is divergence-free in a controlled volume. Before we give a consistent scheme for the current density flux on a cell face, we discretized the Poisson equation (7) on an unstructured mesh. A finite volume representation of the Poisson equation on such a mesh can be written as

$$\frac{1}{\Omega} \oint_S \mathbf{n} \cdot \nabla\varphi \, ds = \frac{1}{\Omega} \sum_{f=1}^{nf} \left(\frac{\partial\varphi}{\partial n} \right)_f s_f = \frac{1}{\Omega} \sum_{f=1}^{nf} \mathbf{n}_f \cdot (\mathbf{u} \times \mathbf{B})_f s_f \tag{20}$$

Considering the situation presented in Fig. 2(a), symbols P and N are used to represent the current cell and neighboring cell in a finite volume computation. The point F is the centroid of the cell face adjoining P and N . \mathbf{l}_f is the unit direction from the cell center P to the neighboring center N , \mathbf{r}_m is the vector line from point F to the middle point of the vector line of PN . Using above notations, the electrical potential gradient on the cell faces can be given as [27]

$$\left(\frac{\partial\varphi}{\partial n} \right)_f = \alpha_f \frac{\varphi_N - \varphi_P}{|x_N - x_P|} + \frac{1}{2} ((\nabla\varphi)_P + (\nabla\varphi)_N) \cdot (\mathbf{n}_f - \alpha_f \mathbf{l}_f) \tag{21}$$

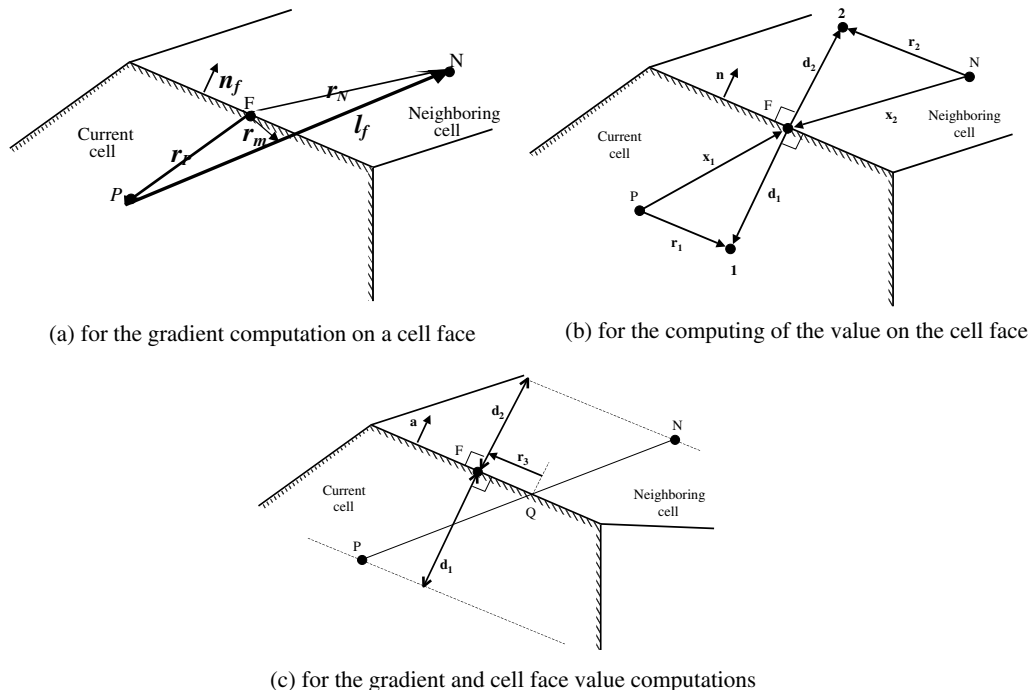


Fig. 2. Vector notation used for non-orthogonal mesh.

$\alpha_f = \mathbf{n}_f \cdot \mathbf{l}_f$ is an optimal value to get an accurate discretization of the gradient at the cell face [27]. The finite volume expression of Eq. (20) can now be expanded in terms of these vectors and the gradient of φ in each cell, as follows:

$$\sum_{f=1}^{nf} \left(\alpha_f \frac{\varphi_N - \varphi_P}{|x_N - x_P|} \right)_f s_f + \sum_{f=1}^{nf} \frac{1}{2} ((\nabla\varphi)_P + (\nabla\varphi)_N)_f \cdot (\mathbf{n}_f - \alpha_f \mathbf{l}_f)_f s_f = \sum_{f=1}^{nf} \mathbf{n}_f \cdot (\mathbf{u} \times \mathbf{B})_f s_f \tag{22}$$

This can be written as an algebraic equation in terms of current cell and neighboring cell quantities, as follows:

$$a_P \varphi_P + \sum_{f=1}^{nf} a_N \varphi_N = S_P \tag{23}$$

While this expression works well and can be used with successive Gauss–Seidel on an orthogonal mesh, the correction term on a non-orthogonal mesh (second term in Eq. (22)) included in the source term S of Eq. (23) would cause it to become numerically unstable. This correction increases the effective stencil size used in the computation, and decreases diagonal dominance of the system of equations. An approach of under-relaxation is to over-relax the diagonal terms by modifying the equation as follows:

$$\frac{a_P \varphi_P}{\alpha} + \sum_{f=1}^{nf} a_N \varphi_N = S_P + \frac{1 - \alpha}{\alpha} a_P \varphi_P \tag{24}$$

$\alpha \in (0, 1]$ is an under-relaxation factor. Eq. (23) is solved by Gauss–Seidel procedure and preconditioned Conjugate Gradient method with good results for Dirichlet boundary conditions and Neumann-type boundary conditions. A numerical stability analysis of the underrelaxation technique for the discretized convective-diffusion equation has been made and the solution stability criterion has been given for under-relaxation technique [28].

A convergent solution of φ , the electrical potential, will be used to conduct the calculation of the current flux on a cell face based on the following formula:

$$(J_n)_f = -\alpha_f \frac{\varphi_N - \varphi_P}{|x_N - x_P|} - \frac{1}{2} ((\nabla\varphi)_P + (\nabla\varphi)_N) \cdot (\mathbf{n}_f - \alpha_f \mathbf{l}_f) + \mathbf{n}_f \cdot (\mathbf{u} \times \mathbf{B})_f \tag{25}$$

Eq. (25) is a consistent scheme for the calculation of the current flux on a cell face, which can conserve the current density. Current density will be divergence-free based on the fluxes from Eq. (25) in a control volume when the electrical potential is obtained from the convergent solution of Eq. (22).

The gradients of the electrical potential at the cell center and its neighbor center, $(\nabla\varphi)_N$ and $(\nabla\varphi)_P$ are needed to accurately calculate the current fluxes on the cell faces. The gradient at a cell center P can be evaluated from Gauss’ rule as

$$(\nabla\varphi)_P = \frac{1}{\Omega_P} \sum_{f=1}^{nf} \varphi_f s_f \mathbf{n}_f \tag{26}$$

To obtain a face interpolation of φ , we first calculate φ_m at the middle point of the vector line of PN as shown in Fig. 2(a) with $\varphi_m = \frac{1}{2}(\varphi_N + \varphi_P)$. In computing face centered quantities, this interpolate must be relocated to the face center F using a local value of gradient and the distance vector \mathbf{r}_m shown in Fig. 2(a). The value of φ at F must be corrected on non-orthogonal meshes where \mathbf{r}_m is non-zero. We estimate this correction from a local interpolated value of the gradient of φ , as follows:

$$\varphi_f = \frac{1}{2}(\varphi_N + \varphi_P) - \frac{1}{2}((\nabla\varphi)_P + (\nabla\varphi)_N) \cdot \mathbf{r}_m \tag{27}$$

Initially, φ_f is estimated from linear interpolation between cell centers. A gradient is computed by Gauss summation over cell faces. This gradient is successively refined by correcting it using the second term in Eq. (27) using the last computed gradient. This process has been seen to converge in four to five steps to near machine zero on several skewed meshes studied.

We would like to list another formula to calculate the electrical potential gradient on the cell faces and the cell center of a control volume [29]. Considering the situation presented in Fig. 2(b), points 1 and 2 are constructed by extending perpendiculars \mathbf{d}_1 and \mathbf{d}_2 from F to intersect the planes parallel to the cell face passing through P and N respectively. Using the above notation, we have $\varphi_1 = \varphi_P + \mathbf{r}_1 \cdot \nabla \varphi_P$, $\varphi_2 = \varphi_N + \mathbf{r}_2 \cdot \nabla \varphi_N$. If the mesh were orthogonal, P and 1 would be the same point, just as N and 2 would be the same. The vectors \mathbf{r}_1 and \mathbf{r}_2 would be zero in an orthogonal mesh and the finite volume representation would be simplified considerably. The vectors \mathbf{x}_1 and \mathbf{x}_2 are distance vectors joining cell centers to face centers in the directions shown. From these vectors, we can compute \mathbf{d}_1 and \mathbf{d}_2 (their normal components) and \mathbf{r}_1 and \mathbf{r}_2 as: $\mathbf{d}_1 = -(\mathbf{x}_1 \cdot \mathbf{n}_f)\mathbf{n}_f$, $\mathbf{d}_2 = -(\mathbf{x}_2 \cdot \mathbf{n}_f)\mathbf{n}_f$, $\mathbf{r}_1 = \mathbf{x}_1 + \mathbf{d}_1$, $\mathbf{r}_2 = \mathbf{x}_2 + \mathbf{d}_2$, and we have

$$\left(\frac{\partial \varphi}{\partial n}\right)_f = \left(\frac{\varphi_2 - \varphi_1}{d_1 + d_2}\right)_f = \underbrace{\left(\frac{\varphi_N - \varphi_P}{d_1 + d_2}\right)_f}_{\text{orthogonal}} + \underbrace{\left(\frac{\mathbf{r}_2 \cdot \nabla \varphi_N - \mathbf{r}_1 \cdot \nabla \varphi_P}{d_1 + d_2}\right)_f}_{\text{non-orthogonal}} \quad (28)$$

d_1 and d_2 are the modules of \mathbf{d}_1 and \mathbf{d}_2 respectively. It includes an orthogonal part and a non-orthogonal correction part.

Using Gauss' law to evaluate the electrical potential gradient at a cell center, we need the value of pressure or electrical potential at the cell faces. Referring to Fig. 2(c), the value of the electrical potential at f can be corrected on non-orthogonal meshes where \mathbf{r}_3 is non-zero. We estimate this correction from a local interpolated value of the gradient of φ , as follows:

$$\varphi_f = \frac{d_2 \varphi_P + d_1 \varphi_N}{d_1 + d_2} + \frac{d_2 (\nabla \varphi)_P + d_1 (\nabla \varphi)_N}{d_1 + d_2} \cdot \mathbf{r}_3 \quad (29)$$

Four to five steps iteration between φ_f and the gradient is needed on several skewed meshes studied. Eq. (28) can then be employed to calculate the current flux using the consistent scheme as

$$(J_n)_f = -\left(\frac{\varphi_N - \varphi_P}{d_1 + d_2}\right)_f - \left(\frac{\mathbf{r}_2 \cdot \nabla \varphi_N - \mathbf{r}_1 \cdot \nabla \varphi_P}{d_1 + d_2}\right)_f + \mathbf{n}_f \cdot (\mathbf{u} \times \mathbf{B})_f \quad (30)$$

3.2. Conservative scheme for calculation of the Lorentz Force

In this subsection, we will develop two techniques to conservatively calculate the Lorentz force. The first one is developed in Section 3.2.1 based on the conservative formulation of the Lorentz force. The second one is developed in Section 3.2.2 based on a conservative interpolation of the current density at the cell center from the cell faces of a controlled volume. The conservative current density at the cell center will be used to calculate the Lorentz force. These two techniques are equivalent when the applied magnetic field is constant, and both can conserve the total momentum from the Lorentz force.

3.2.1. Based on a conservative formula of the Lorentz force

Now the conservative current fluxes on the cell faces will be used to conduct the calculation of the Lorentz force in a control volume. Applied Eq. (11) on a controlled volume Ω_c , we have

$$\int_{\Omega_c} \mathbf{J} \times \mathbf{B} d\Omega = - \int_{\Omega_c} \nabla \cdot (\mathbf{J}(\mathbf{B} \times \mathbf{r})) d\Omega + \int_{\Omega_c} \nabla \cdot (\mathbf{J}\mathbf{B}) \times \mathbf{r} d\Omega \quad (31)$$

The terms at the right hand side of Eq. (31) can then be approximated as

$$\Omega_c(\nabla \cdot (\mathbf{J}(\mathbf{B} \times \mathbf{r})))_c = \int_{\Omega_c} \nabla \cdot (\mathbf{J}(\mathbf{B} \times \mathbf{r})) d\Omega = \oint_S \mathbf{n} \cdot (\mathbf{J}(\mathbf{B} \times \mathbf{r})) ds = \sum_{f=1}^{nf} (J_n)_f (\mathbf{B} \times \mathbf{r})_f s_f \quad (32)$$

$$\Omega_c(\nabla \cdot (\mathbf{J}\mathbf{B}) \times \mathbf{r})_c = \Omega_c(\nabla \cdot (\mathbf{J}\mathbf{B}))_c \times \mathbf{r}_c = \int_{\Omega_c} \nabla \cdot (\mathbf{J}\mathbf{B}) d\Omega \times \mathbf{r}_c = \oint_S \mathbf{n} \cdot (\mathbf{J}\mathbf{B}) ds \times \mathbf{r}_c = -\mathbf{r}_c \times \sum_{f=1}^{nf} (J_n)_f \mathbf{B}_f s_f \quad (33)$$

Therefore, we have the following approximation of Eq. (31) as:

$$(\mathbf{J} \times \mathbf{B})_c = -(\nabla \cdot (\mathbf{J}\mathbf{B} \times \mathbf{r}))_c + (\nabla \cdot (\mathbf{J}\mathbf{B}))_c \times (\mathbf{r})_c \tag{34}$$

In detail, we have

$$(\mathbf{J} \times \mathbf{B})_c = -\frac{1}{\Omega_c} \sum_{f=1}^{nf} (\mathbf{J}_n)_f (\mathbf{B} \times \mathbf{r})_f s_f - \mathbf{r}_c \times \frac{1}{\Omega_c} \sum_{f=1}^{nf} (\mathbf{J}_n)_f \mathbf{B}_f s_f \tag{35}$$

The subscript *c* denotes the cell center. In this scheme, the Lorentz force at the cell center has been calculated based on the conservative formula of Eq. (11). When the applied magnetic field is constant, the second term on the right hand side of Eq. (35) will disappear since a consistent scheme has been employed to ensure the divergence free of current density in a control volume. In other words, the consistent scheme can ensure $\sum_{f=1}^{nf} (\mathbf{J}_n)_f s_f = 0$ to near machine precision. The total momentum contribution from the Lorentz force only depends on the boundary conditions and is conservative using Eq. (35) to conduct the calculation of the Lorentz force. Moreover, the calculation of the Lorentz force in a control volume using Eq. (35) only needs the current fluxes on the cell faces. Any interpolation to obtain the current density at the cell center from the current fluxes on the cell faces is not needed. It is convenient and useful to use the conservative formula of Eq. (35) to reduce the numerical error from the interpolation. When the applied magnetic field is spatially varying, the total momentum due to the contribution of the Lorentz force is not conservative. The second-term on the right hand side of Eq. (35) is a first-order approximation of Eq. (11) since \mathbf{r}_c has been moved out of the integral formula of Eq. (31).

3.2.2. Based on a conservative interpolation of current density

To direct calculate the Lorentz force at the cell center based on a non-conservative formulation of $\mathbf{J}_c \times \mathbf{B}_c$, we need the current density at the cell center by an interpolation from the current fluxes on the cell faces. The simple interpolation in [14] can get accurate results for MHD at high Hartmann numbers on a rectangular collocated mesh. A straight forward extension of the simple interpolation on an unstructured mesh can be given as

$$(j_x)_c = \frac{\sum_{f=1}^{nf} (j_x |s_x|)_f}{\sum_{f=1}^{nf} |s_x|_f}, \quad (j_y)_c = \frac{\sum_{f=1}^{nf} (j_y |s_y|)_f}{\sum_{f=1}^{nf} |s_y|_f}, \quad (j_z)_c = \frac{\sum_{f=1}^{nf} (j_z |s_z|)_f}{\sum_{f=1}^{nf} |s_z|_f} \tag{36}$$

where $\mathbf{s} = (s_x, s_y, s_z)$ is the dimensional face normal area vector with $s_f = \sqrt{(s_x)^2 + (s_y)^2 + (s_z)^2}$. The interpolation of Eq. (36) is based on an area average. This average can conserve the current density only on a rectangular collocated mesh. Indeed, Eq. (36) will be reduced to the conservative interpolation scheme on a rectangular grid system in [14], which can conduct the MHD calculation at high Hartmann numbers with good accuracy. However the scheme of Eq. (36) cannot conserve the total momentum on a skewed mesh when the applied magnetic field is constant. This interpolation introduces numerical error for the calculation of the Lorentz force on a skewed mesh.

When the applied magnetic field is constant, the conservative formulation of the Lorentz force can be given as

$$\mathbf{J} \times \mathbf{B} = \nabla \cdot (\mathbf{J}(\mathbf{r} \times \mathbf{B})) = \nabla \cdot (\mathbf{J}\mathbf{r}) \times \mathbf{B} \tag{37}$$

$\nabla \cdot (\mathbf{J}\mathbf{r})$ can be regarded as an interpolation of the current density. In fact, since the current density is conservative with $\nabla \cdot \mathbf{J} = 0$, we have following equation for the current density:

$$\mathbf{J} = \nabla \cdot (\mathbf{J}\mathbf{r}) \tag{38}$$

Therefore, no matter the applied magnetic field is constant or not, the Lorentz force can be expressed as

$$\mathbf{J} \times \mathbf{B} = (\nabla \cdot (\mathbf{J}\mathbf{r})) \times \mathbf{B} \tag{39}$$

Eq. (39) returns to the conservative formula of the Lorentz force in Eq. (11) when the applied magnetic field is spatial invariant, which can conserve the total momentum due to the contribution of the Lorentz force. Eq. (38) can be used to interpolate the current density at the cell center from the current fluxes at cell faces. The detailed discretized formulation is

$$\mathbf{J}_c = \frac{1}{\Omega_c} \int_{\Omega_c} \mathbf{J} d\Omega = \frac{1}{\Omega_c} \int_{\Omega_c} \nabla \cdot (\mathbf{J}\mathbf{r}) d\Omega = \frac{1}{\Omega_c} \oint_{S_c} J_n \mathbf{r} ds = \frac{1}{\Omega_c} \sum_{f=1}^{nf} (J_n)_f \mathbf{r}_f s_f \tag{40}$$

Corresponding to the non-conservative interpolation of Eq. (36), the conservative interpolation of Eq. (40) can be rewritten as

$$(j_x)_c = \frac{1}{\Omega_c} \sum_{f=1}^{nf} (J_n)_f s_f x_f, \quad (j_y)_c = \frac{1}{\Omega_c} \sum_{f=1}^{nf} (J_n)_f s_f y_f, \quad (j_z)_c = \frac{1}{\Omega_c} \sum_{f=1}^{nf} (J_n)_f s_f z_f \tag{41}$$

Unlike the non-conservative interpolation of Eq. (36), which is based on an area average, the conservative interpolation of Eq. (40) is based on a volume average. In fact, Eq. (40) can be discretized in a different way as

$$\mathbf{J}_c = \frac{1}{\Omega_c} \int_{\Omega_c} \nabla \cdot (\mathbf{J}(\mathbf{r} - \mathbf{r}_c)) d\Omega = \frac{1}{\Omega_c} \oint_{S_c} J_n (\mathbf{r} - \mathbf{r}_c) ds = \frac{1}{\Omega_c} \sum_{f=1}^{nf} (J_n)_f (\mathbf{r}_f - \mathbf{r}_c) s_f \tag{42}$$

Considering a circum-center based unstructured grid as shown in Fig. 3. We have

$$\mathbf{r}_f - \mathbf{r}_c = d_f \mathbf{n}_f \tag{43}$$

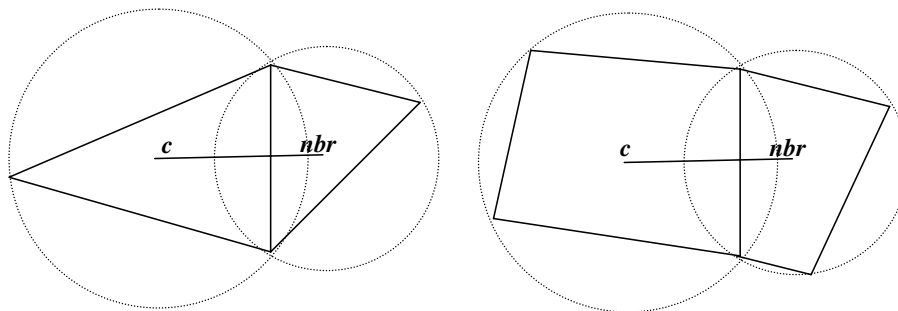
Here, d_f denotes the distance from the cell center to the cell face. Substitute Eq. (43) into Eq. (42), we, therefore, have

$$\mathbf{J}_c = \frac{1}{\Omega_c} \sum_{f=1}^{nf} (J_n)_f d_f s_f \mathbf{n}_f \tag{44}$$

For a circum-center hexahedral or tetrahedral grid, we have $\Omega_c = \sum_{f=1}^{nf} \frac{1}{3} s_f d_f$. Eq. (44) is, in fact, a volume average of $(J_n)_f \mathbf{n}_f$. When the grid is rectangular, we have $\frac{s_f d_f}{\Omega_c} = \frac{1}{2}$, and Eq. (44) can be reduced as

$$\mathbf{J}_c = \sum_{f=1}^{nf} (J_n)_f \frac{s_f d_f}{\Omega_c} \mathbf{n}_f = \frac{1}{2} \sum_{f=1}^{nf} (J_n)_f \mathbf{n}_f \tag{45}$$

This is the simple interpolation scheme we used for the calculation of the current density at the cell center from the current fluxes at the cell faces in [14], which means the simple interpolation in [14] meets the conservative condition of $\nabla \cdot \mathbf{J} = 0$ and $\mathbf{J} = \nabla \cdot (\mathbf{J}\mathbf{r}) = 0$. The Lorentz force's calculation using this simple interpolation is equivalent to the discretized conservative formulation of Eq. (35) on a rectangular grid with constant applied magnetic field, in which the Lorentz force is in a conservative form. Therefore, the total momentum contribution from the Lorentz force using the simple interpolation on a rectangular grid [14] is conservative. The simple interpolation can be used to simulate MHD at high Hartmann numbers with good accuracy on a rectangular mesh as shown in [14].



(a) Circumcenter triangular grid

(b) Circumcenter quadrilateral grid

Fig. 3. Schematic circum-center grid.

3.3. A non-conservative scheme for calculation of the Lorentz force

The current density at the cell center is needed to directly calculate the Lorentz force at the cell center based on a non-conservative formulation of $\mathbf{J}_c \times \mathbf{B}_c$. Section 3.2.2 gives a way to get the current density at the cell center conservatively interpolated from the current fluxes on the cell faces. The current density at the cell center can also be directly calculated from the gradient of electrical potential and velocity at the cell center based on Ohm’s law as

$$\mathbf{J}_c = -(\nabla\varphi)_c + (\mathbf{u} \times \mathbf{B})_c \tag{46}$$

The gradient of the electrical potential $(\nabla\varphi)_c$ at the cell center will be calculated based on the Gauss’ rule as described in Eq. (26). φ_f can be iteratively calculated using Eq. (27). We then have the detailed formula for the calculation of the current density at the cell center as

$$\mathbf{J}_c = -\frac{1}{\Omega_c} \sum_{f=1}^{nf} \varphi_f s_f \mathbf{n}_f + \mathbf{u}_c \times \mathbf{B}_c \tag{47}$$

The Lorentz force will be calculated based on the current density using Eq. (47) as

$$(\mathbf{J} \times \mathbf{B})_c = \mathbf{J}_c \times \mathbf{B}_c = \left(-\frac{1}{\Omega_c} \sum_{f=1}^{nf} \varphi_f s_f \mathbf{n}_f + \mathbf{u}_c \times \mathbf{B}_c \right) \times \mathbf{B}_c \tag{48}$$

As we have analyzed for a rectangular mesh [14], the current density calculated using Eq. (47) and the Lorentz force calculated based on Eq. (48) are not conservative. In fact, the Lorentz force calculated using Eq. (48) cannot conserve the total momentum when the applied magnetic field is constant. This non-conservative current density from Eq. (47) cannot be used to accurately calculate the Lorentz force, and it will introduce a numerical error for the calculation of the total momentum.

4. Projection method and detailed calculation procedures for MHD

A general second-order temporal accuracy of projection method [30] has been extended for MHD flows [14]. We now summarize the consistent and conservative schemes developed for an unstructured collocated mesh, and give a detailed computation procedure for MHD flows based on the general four-step projection method in [14]. For the sake of the simulations of MHD flows with solid walls included, we will describe our detailed computational procedure based on the dimensional incompressible MHD equations with variable coefficients. The dimensional incompressible Navier–Stokes equations and Ohm’s law with variable coefficients can be given here as

$$\frac{\partial \mathbf{u}}{\partial t} + \mathbf{u} \cdot \nabla \mathbf{u} = \frac{1}{\rho} (-\nabla p + \nabla \cdot (\eta \nabla \mathbf{u}) + (\mathbf{J} \times \mathbf{B})) \tag{49}$$

$$\mathbf{J} = \sigma (-\nabla \varphi + \mathbf{u} \times \mathbf{B}) \tag{50}$$

Based on the dimensional Navier–Stokes equation and continuity equation, the first predictor step can be given as

$$\frac{\hat{\mathbf{u}}_c - \mathbf{u}_c^k}{\Delta t} = -(\mathbf{u} \cdot \nabla \mathbf{u})_c^{k+1/2} + \frac{1}{\rho_c^{k+1/2}} (\nabla \cdot (\eta \nabla \mathbf{u}))_c^{k+1/2} + \frac{1}{\rho_c^k} \left(-\nabla_c(p_c^k) + (\mathbf{J} \times \mathbf{B})_c^k \right) \tag{51}$$

The superscript k denotes the k th time level. The convective term is updated as $-(\mathbf{u} \cdot \nabla \mathbf{u})_c^{k+1/2}$ and the diffusion term is updated as $(\nabla \cdot (\eta \nabla \mathbf{u}))_c^{k+1/2} / \rho_c^{k+1/2}$. Usually an explicit Runge–Kutta technique can be employed for update of the convective term for simplicity, and an implicit technique is used for update of the diffusion term for stability. In our simulation, we use the semi-implicit Crank–Nicholson scheme to update both the convective term and the diffusion term. When the semi-implicit Crank–Nicholson scheme is employed, we have the update of the diffusion term as

$$\frac{1}{\rho_c^{k+1/2}} (\nabla \cdot (\eta \nabla \mathbf{u}))_c^{k+1/2} = \frac{1}{2} \left(\frac{1}{\rho_c^{k+1}} (\nabla \cdot (\eta \nabla \mathbf{u}))_c^{k+1} + \frac{1}{\rho_c^k} (\nabla \cdot (\eta \nabla \mathbf{u}))_c^k \right)$$

The second predictor velocity at the cell center can be given using the following equation:

$$\tilde{\mathbf{u}}_c = \hat{\mathbf{u}}_c + \Delta t \Theta_c^k \frac{1}{\rho_c^k} \nabla_c (p_c^k) \quad (52)$$

Here $\Theta^k = \text{diag}(\theta_x^k, \theta_y^k, \theta_z^k)$ is a diagonal coefficient matrix with elements $\theta_x^k, \theta_y^k, \theta_z^k$, which may depend on the grid size, time step and even velocity [30]. Usually, we employ the same scheme to discretize the convective terms and/or the diffusion terms for the x -directional, y -directional, and z -directional momentum equations. We then have $\theta_x^k = \theta_y^k = \theta_z^k = \theta^k$, and $\Theta^k = \theta^k \mathbf{I}$. Here, \mathbf{I} is the unit matrix. In this paper, we only consider the projection method with $\Theta^k = \theta^k \mathbf{I}$, and Eq. (52) can be reduced as

$$\tilde{\mathbf{u}}_c = \hat{\mathbf{u}}_c + \Delta t \theta_c^k \frac{1}{\rho_c^k} \nabla_c (p_c^k) \quad (53)$$

The predictor velocity fluxes on the cell faces can then be obtained by interpolation from the second predictor velocities at the cell centers

$$\tilde{U}_f = \tilde{\mathbf{u}}_f \cdot \mathbf{n}_f = \overline{\tilde{\mathbf{u}}_c} \cdot \mathbf{n}_f \quad (54)$$

$\overline{\tilde{\mathbf{u}}_c}$ represents an average or interpolation from the velocity $\tilde{\mathbf{u}}_c$ at the neighboring cell centers of the face f to the velocity $\tilde{\mathbf{u}}_f$ on the face f . The similar technique as that for φ_f in Eq. (27) can be used to get the $\tilde{\mathbf{u}}_f$. The predictor velocity fluxes on the cell faces of a control volume are used to calculate the source term of the pressure Poisson equation which is solved to get the pressure at the next time level. Using the Gauss' rule, the discretized Poisson equation can then be written as

$$\Delta t \sum_{f=1}^{nf} \theta_f^k \frac{1}{\rho_f^{k+1}} \left(\frac{\partial p_c^{k+1}}{\partial n} \right)_f s_f = \sum_{f=1}^{nf} \tilde{U}_f s_f \quad (55)$$

In this discretized pressure Poisson equation, pressure gradients at cell faces along the normal directions and predictor velocity's fluxes are needed. From Eq. (55), the pressure at the time level of $k+1$ is obtained, which is used to calculate the normal pressure gradient on the cell faces based on either Eq. (21) or (28). The normal pressure gradient at the cell face is used to conduct the calculation of the velocity flux at time level $k+1$ using the following equation:

$$U_f^{k+1} = \tilde{U}_f - \Delta t \theta_f^k \frac{1}{\rho_f^{k+1}} \left(\frac{\partial p_c^{k+1}}{\partial n} \right)_f \quad (56)$$

The velocity of the time level $k+1$ at a cell center is calculated from the following equation:

$$\mathbf{u}_c^{k+1} = \tilde{\mathbf{u}}_c - \Delta t \theta_c^k \frac{1}{\rho_c^{k+1}} \nabla_c (p_c^{k+1}) \quad (57)$$

where the pressure gradient of $\nabla_c (p_c^{k+1})$ at the cell center is calculated based on Gauss' rule. The velocities at cell centers from Eq. (57) can then be used to get the velocity at a cell face by an interpolation

$$\mathbf{u}_f^{k+1} = \overline{\mathbf{u}_c^{k+1}} \quad (58)$$

$\overline{\mathbf{u}_c^{k+1}}$ denotes an average or interpolation from the velocity \mathbf{u}_c^{k+1} at the neighbor cell centers of the face f to the velocity \mathbf{u}_f^{k+1} on the face f . The similar technique as that for φ_f in Eq. (27) can be used to get the \mathbf{u}_f^{k+1} . This velocity is then used to calculate

$$(\mathbf{u} \times \mathbf{B})_f^{k+1} = \mathbf{u}_f^{k+1} \times \mathbf{B}_f^{k+1} \quad (59)$$

and the discretized electrical potential Poisson equation can be given in a controlled volume using the Gauss' rule as

$$\sum_{f=1}^{nf} \sigma_f \left(\frac{\partial \varphi_c^{k+1}}{\partial n} \right)_f s_f = \sum_{f=1}^{nf} \sigma_f (\mathbf{u} \times \mathbf{B})_f^{k+1} \cdot \mathbf{n}_f s_f \quad (60)$$

The current flux on a cell face can then be calculated using the consistent scheme based on the Ohm's law

$$(J_n)_f^{k+1} = \sigma_f \left(- \left(\frac{\partial \varphi_c^{k+1}}{\partial n} \right)_f + (\mathbf{u} \times \mathbf{B})_f^{k+1} \cdot \mathbf{n}_f \right) \quad (61)$$

The consistent scheme requires that $\left(\frac{\partial \varphi_c^{k+1}}{\partial n} \right)_f$ in Eqs. (60) and (61) is discretized using the same scheme. Eq. (21) and/or (28) can be used to discretize $\left(\frac{\partial \varphi_c^{k+1}}{\partial n} \right)_f$ with a second-order spatial accuracy.

The Lorentz force will be calculated using the following three schemes:

- Based on the divergence form of the Lorentz force of Eq. (35)

$$(\mathbf{J} \times \mathbf{B})_c^{k+1} = - \frac{1}{\Omega_c} \sum_{f=1}^{nf} (J_n)_f^{k+1} (\mathbf{B}_f^{k+1} \times \mathbf{r}_f) s_f - \mathbf{r}_c \times \frac{1}{\Omega_c} \sum_{f=1}^{nf} (J_n)_f^{k+1} \mathbf{B}_f^{k+1} s_f \quad (62)$$

- Based on the conservative interpolation of Eq. (42)

$$(\mathbf{J} \times \mathbf{B})_c^{k+1} = \left(\frac{1}{\Omega_c} \sum_{f=1}^{nf} (J_n)_f^{k+1} (\mathbf{r}_f - \mathbf{r}_c) s_f \right) \times \mathbf{B}_c^{k+1} \quad (63)$$

- Based on the non-conservative scheme developed in Eq. (48)

$$(\mathbf{J} \times \mathbf{B})_c^{k+1} = \sigma_c \left(- \frac{1}{\Omega_c} \sum_{f=1}^{nf} \varphi_f s_f \mathbf{n}_f + \mathbf{u}_c \times \mathbf{B}_c \right) \times \mathbf{B}_c \quad (64)$$

It is already shown in [14,30] that some classical projection methods [31,32] can be acquired from the general projection method with a different coefficient matrix. And SIMPLE [33] and SIMPLEC [34] methods can also be acquired from the general projection method with a nonlinear coefficient matrix, which is dependent on velocity, grid size and time step. The SIMPLE and SIMPLEC methods have been proven to have second-order temporal accuracy [35]. On the collocated mesh, the technique developed in [36] is applied for the general projection method to overcome the checkboard phenomena of pressure.

The boundary conditions for the projection method with the Lorentz force included have been given in [14]. The second-order temporally accurate velocity boundary condition for the predictor-step of Eq. (51) is

$$\hat{\mathbf{u}}_{BC} = \mathbf{u}_{BC}^{k+1} \quad (65)$$

and the pressure boundary conditions for the pressure Poisson equation of Eq. (55) is

$$\left(\frac{\partial p_c^{k+1}}{\partial n} \right)_{BC} = \left(\frac{\partial p_c^k}{\partial n} \right)_{BC} \quad (66)$$

The complete algorithm from time step k to time step $k + 1$ can be summarized based on the four-step projection method on a collocated mesh as:

- (1) Evaluate Lorentz force $(\mathbf{J} \times \mathbf{B})_c^k$ at time level k using a scheme from Eqs. 62, 63, 63, and calculate the pressure gradient $\nabla_c(p_c^k)$ at the cell center using the Gauss' rule.
- (2) Evaluate coefficient θ_c^k and θ_f^k (here we choose $\theta_c^k = 1$ and $\theta_f^k = 1$).
- (3) Solve the predictor step of Eq. (51) for $\hat{\mathbf{u}}_c$ with the boundary conditions from Eq. (65); obtain the second intermediate velocity $\tilde{\mathbf{u}}_c$ using Eq. (53); transfer the cell center velocity $\tilde{\mathbf{u}}_c$ to the face center velocity $\tilde{\mathbf{u}}_f$ using $\tilde{\mathbf{u}}_f = \tilde{\mathbf{u}}_c$ and calculate the velocity flux \tilde{U}_f on the cell faces of a control volume using Eq. (54).

- (4) Solve the pressure Poisson equation of Eq. (55) for p_c^{k+1} using the preconditioned conjugate gradient method with the boundary conditions from Eq. (66); calculate $\nabla_c(p_c^{k+1})$ using Eq. (26) and $\left(\frac{\partial p_c^{k+1}}{\partial n}\right)$ using Eq. (21) or (28).
- (5) Correct the velocity \mathbf{u}_c^{k+1} at cell center based on $\tilde{\mathbf{u}}_c$ and $\nabla_c(p_c^{k+1})$ using Eq. (57); correct the velocity flux at the face center based on \tilde{U}_f and $\left(\frac{\partial p_c^{k+1}}{\partial n}\right)$ using Eq. (56), calculate the cell face velocity based on the neighboring centers' velocity using $\mathbf{u}_f^{k+1} = \overline{\mathbf{u}_c^{k+1}}$ of Eq. (58).
- (6) Calculate $(\mathbf{u} \times \mathbf{B})_f^{k+1}$ using Eq. (59); solve the electrical potential Poisson equation (60) for ϕ_c^{k+1} using the preconditioned conjugate gradient method.
- (7) Calculate $\left(\frac{\partial \phi_c^{k+1}}{\partial n}\right)$ using Eq. (21) or (28) and calculate the current density flux of $(J_n)_f^{k+1}$ at the cell face using the corresponding consistent scheme of Eq. (25) or (30); calculate the gradient of the electrical potential $\nabla_c(\phi_c^{k+1})$ at the cell center using Eq. (26).
- (8) Calculate Lorentz force of $(\mathbf{J} \times \mathbf{B})_c^{k+1}$ at the cell center based on the conservative formula of Eq. (62) or the conservative interpolation of Eq. (63) or the non-conservative interpolation of Eq. (64).
- (9) Repeat above steps from (2) to (8) by setting $k = k + 1$ for the next time level.

The above projection method can balance the pressure term and the Lorentz force in the fully developed core flow when the conservative formula of Eq. (62) or the conservative interpolation of Eq. (63) are employed to calculate the Lorentz force. The consistent and conservative scheme developed in this paper is used to calculate the Lorentz force at the cell center. This includes the calculation of current density fluxes at the cell faces using a consistent scheme, which will ensure the divergence free of current density, and the calculation of the Lorentz force based on the conservative formula of Eq. (62) or the conservative interpolation of Eq. (63). We will numerically show that the non-conservative scheme of Eq. (64) cannot get accurate results.

5. Validation of consistent and conservative schemes

There exist some exact solutions for fully developed incompressible laminar flows in ducts with transverse magnetic fields. Shercliff's solution for rectangular ducts with non-conducting walls and the field perpendicular to one side [6] and Hunt's solution for rectangular ducts with two non-conductive side walls and two conductive Hartmann walls [7] have been used to validate the consistent and conservative scheme developed for rectangular grids in [14]. These solutions are also used to validate the consistent and conservative schemes developed here for an unstructured mesh with skewed grids. Shercliff's case will be simulated on an orthogonal mesh with core perturbation. Hunt's case will be simulated on a triangular mesh and a prism mesh. Hunt's formula has been reformulated in Appendix A for the sake of numerical calculation using a computer code at high Hartmann numbers without further approximation. Considering that Shercliff's case is a special case of Hunt's case, the reformulated Hunt's formula can also be used to get the exact solution for Shercliff's case. Experimental data for a 3D circular pipe flow in a spatially variable magnetic field is used to further validate the scheme on a fully three-dimensional unstructured mesh.

5.1. Conservation of current density

5.1.1. Shercliff's case on a rectangular mesh with core perturbation

We simulate Shercliff's case of a fully developed flow in a square channel with all of the walls electrically insulated. We present some preliminary results from a fully developed flow calculation on an orthogonal mesh with core perturbation (Fig. 4(a)) at $Ha = 300$ and $Re = 10$ with a pressure gradient of -31.662 specified, which corresponds to a mass flow rate of 4 from Shercliff's solution.

On rectangular grids, this case has been simulated with good accuracy by using the consistent and conservative scheme in [14]. On the mesh of Fig. 4(a) with core perturbation, the consistent scheme is used to conduct the calculation of the current fluxes on the cell faces, which meet the condition of the divergence free of the current density in a controlled volume. The Lorentz force is calculated based on the conservative formulation of Eq. (62) represented as "NGRAD = 5", the simple interpolation of Eq. (36) represented as

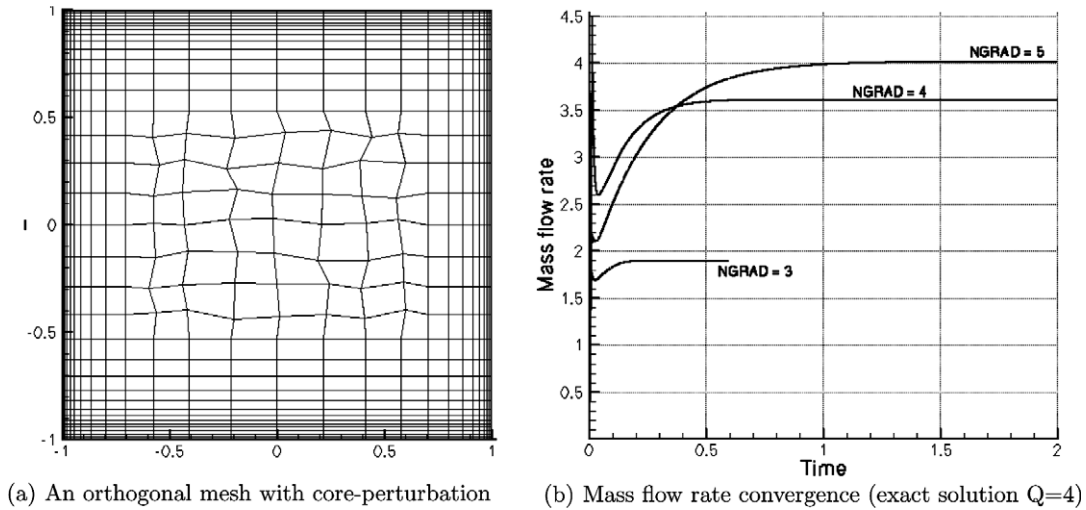


Fig. 4. Shercliff’s case with $Ha = 300$ on an orthogonal mesh with core-perturbation.

“NGRAD = 4”, and the non-conservative scheme of Eq. (64) represented as “NGRAD = 3” in Fig. 4(b). Fig. 4(b) tells us the Lorentz force calculated based on the conservative formulation of Eq. (62) can be used to get an accurate result, which matches well with the analytical results on the skewed grids. However, the simple interpolation of Eq. (36) cannot get an accurate result for MHD even at $Ha = 300$; while the Lorentz force from the non-conservative scheme of Eq. (64) gives the value of flow rate with the most deviation from the actual result as shown in Fig. 4(b) and lowest velocity distribution.

Let us give a detailed analysis on these results. The simple interpolation of Eq. (36) is equivalent to the conservative interpolation of Eq. (63) on a rectangular grid. However, on a skewed grid, the simple interpolation of Eq. (36) cannot conserve the current. In other words, the simple interpolation can conserve the current near the boundary with rectangular grids used there but not at the core with skewed grids used. The non-conservative current at the core will introduce numerical errors on the calculation of the Lorentz force there. The inaccurate Lorentz force cannot effectively balance the pressure gradient at the core, which should be balanced as shown in Eq. (2). The flow rate as shown in Fig. 4(b) cannot be accurately calculated due to the imbalance between the Lorentz force and the pressure gradient at the core. The non-conservative scheme of Eq. (64) cannot conserve current at any kind of grid, which will introduce numerical errors for the calculation of the Lorentz force at the whole computation region. Therefore, the non-conservative scheme gives the worst result as shown in Fig. 4(b).

For the constant applied magnetic field, calculation of the Lorentz force using the conservative interpolation of Eq. (63) can get the same accurate result as that from the conservative formulation of Eq. (62).

5.1.2. Hunt’s case on a triangular mesh and a prism mesh

We now consider the fully developed flow in a square channel with $Re = 10$, $Ha = 300$ of the Hunt’s case. The walls perpendicular to the applied magnetic field are assumed to be conducting with a wall conductance ratio $c_w = 0.05$ and those parallel to the applied magnetic field are electrically insulated. The pressure gradient is given as -374.897 , which corresponds to the mass flow rate of 4 based on the Hunt’s analytical solution. In the numerical result, the presented consistent scheme is used to conduct the calculation of the current fluxes on the cell faces. The Lorentz force is calculated based on the conservative formulation of Eq. (62). The Lorentz force can also be calculated based on the conservative interpolation of Eq. (63).

A triangular mesh is generated with fine grids in the side layers and finer grids in the Hartmann layers. In detail, the mesh in the two times thickness of Hartmann layers is resolved with cells having minimum size $1/(3Ha)$, and maximum size $1/Ha$. The mesh in the 2.5 times thickness of the side layers is resolved with cells having minimum size $1/(3Ha^{1/2})$, and maximum size $1/Ha^{1/2}$. The mesh is shown in Fig. 5(a). With a close

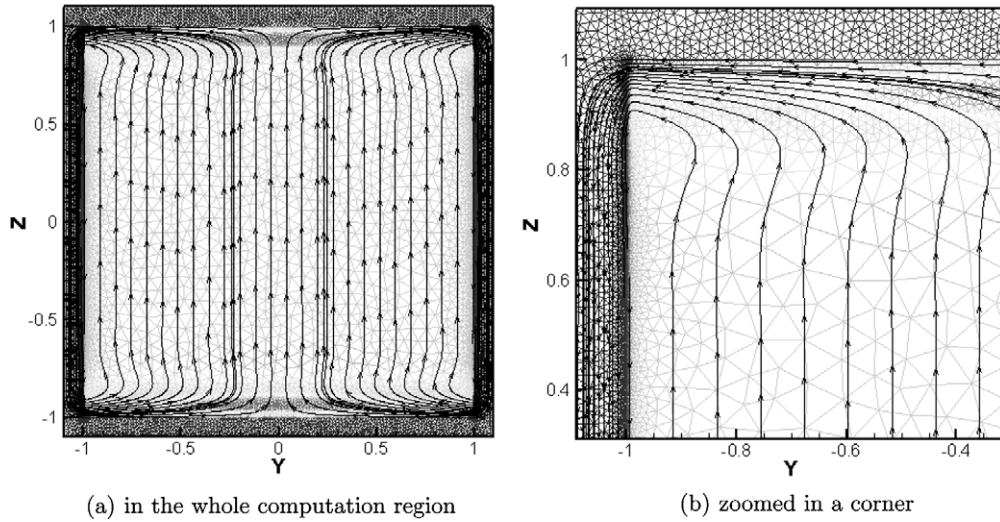


Fig. 5. Vector notation used for non-orthogonal mesh.

look at the grids near a corner as shown in Fig. 5(b), we can clearly see that the grids are non-uniform with coarse grids in the core, fine grids in the side layer and finer grids in the Hartmann layer.

The iteration history of divergence of the current density is shown in Fig. 6. The consistent scheme used in the calculation can keep the calculated current fluxes conserved since the maximum divergence of the current calculated based on the fluxes in a control volume is reduced as time marching. The flow rate converges to the exact value of 4 with an error less than 1% when it reaches the convergent result as shown in Fig. 6(b). The streamlines of current at cell centers illustrated in Fig. 5(a) and (b) are closed, which shows that the current at the cell center calculated using the conservative interpolation of Eq. (42) is conservative. This conservative current can be used to calculate the Lorentz force at the cell center with good accuracy.

Velocity distributions calculated on the triangular grid using the consistent and conservative scheme are shown in Fig. 7(a). We present a comparison between the exact solution from the Hunt's analysis and the numerical solution in Fig. 7(b). This figure illustrates the comparison in the Hartmann layers and side layers. The results on triangular mesh match the analytical results well. The comparison demonstrates a very good computational accuracy.

Numerical simulation is also done for the fully developed flow with $Ha = 1000$. The pressure gradient is given as -1000 . The triangle mesh is refined in the two times thickness of Hartmann layers with minimum

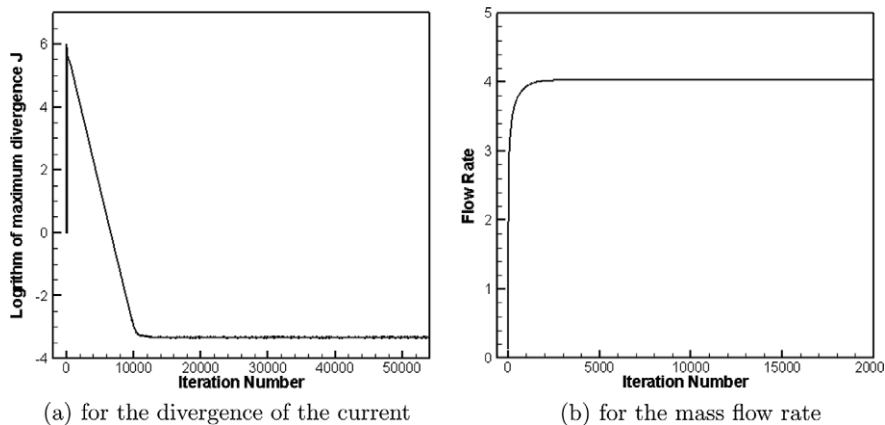


Fig. 6. Convergent history for the calculation of $Ha = 300$.

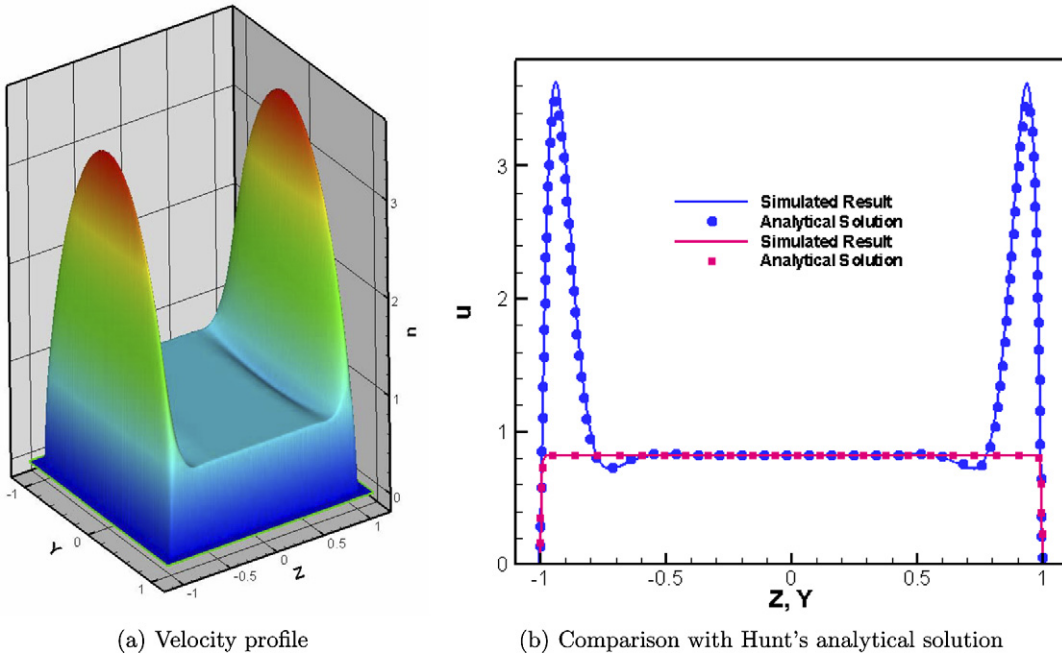


Fig. 7. Calculated velocity for $Ha = 300$.

size $1/(3Ha)$, and maximum size $1/Ha$. The mesh is also refined in the 3 times thickness of the side layers with minimum size $1/(3Ha^{1/2})$, and maximum size equal to $1/Ha^{1/2}$. The comparison between the numerical results and the Hunt's analytical solution is illustrated in Fig. 8. Fig. 8(a) presents the comparison of the velocity along the middle line normal to the Hartmann walls. Fig. 8(b) presents the comparison of the velocity along the middle line normal to the side walls. The numerical results match well with the analytical results. The velocity profile and the current distribution are given in Fig. 9. Fig. 9(b) clearly shows the calculated current is conservative on the triangular mesh.

From the simulations for the fully developed MHD flows of the Shercliff's case and the Hunt's case in a duct, we can conclude that the consistent scheme can keep the calculated current fluxes divergence free on

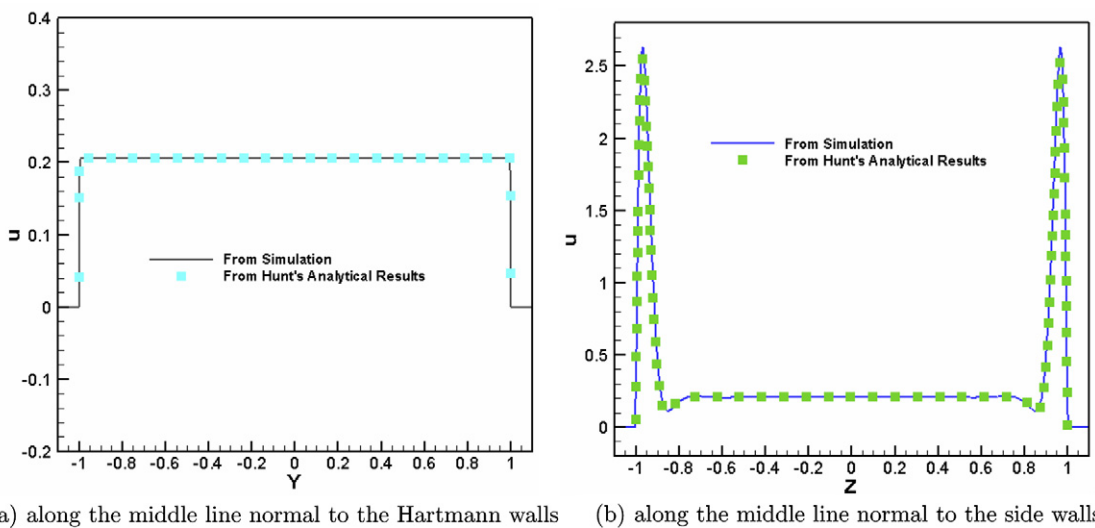


Fig. 8. Comparison with Hunt's analytical solution for $Ha = 1000$.

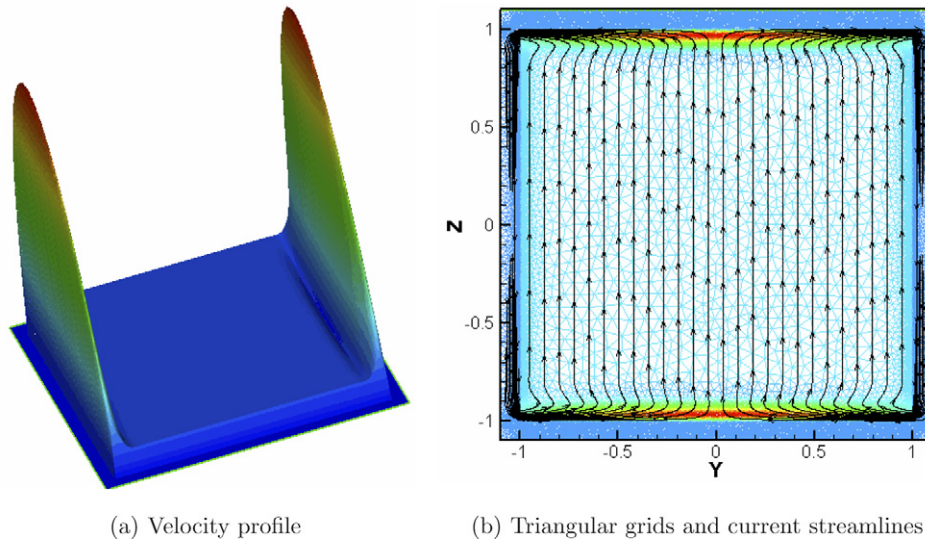


Fig. 9. Velocity profile and current streamlines for $Ha = 1000$ on a triangular mesh.

an arbitrary unstructured mesh. The divergence-free current flux can be used to conduct the calculation of the Lorentz force using the conservative formula of Eq. (62). It also can be used to get the conservative current density at the cell center using the conservative interpolation of Eq. (42). The current density at the cell center using the conservative interpolation can be further employed to calculate the Lorentz force using Eq. (63). The Lorentz force calculated using the conservative formula of Eq. (62) and conservative interpolation of Eq. (63) can balance the pressure gradient in the fully developed core flow on an arbitrary unstructured mesh. The Lorentz force calculated using the conservative method can conserve the total momentum supposing the applied magnetic field is constant, which can ensure the simulated results accurate on an arbitrary mesh. The non-conservative scheme of Eq. (64) cannot ensure the total momentum contributed from the Lorentz force is conservative. The non-conservative Lorentz force from Eq. (64) cannot give an accurate prediction for MHD flows. Also it has been shown that the simple interpolation of Eq. (36) cannot conserve the current density at the cell center on a skewed grid, although it can conserve the current on a rectangular grid.

It is of interest to test our approach in a three-dimensional simulation with different interaction parameters. We choose here the same cross section as above and extend it in the x -direction to 30 units (channel half-width is 1). An unstructured prism mesh was used in this simulation with the mesh in a cross section same as that we generated for 2D fully developed MHD flows. The mesh number in the flow direction is 31. The 3D prism mesh is partitioned to run on 16 different processors.

A bi-parabolic inflow velocity distribution with flow rate of 4 is given and used as an initial flow condition in the channel. Magnetic field with a value of 1 is applied in the y -direction. The flow quickly adjusts from ordinary laminar flow profile to the fully developed MHD state, converges rapidly and is virtually indistinguishable from the exact solution. With $Ha = 300$ and $c_w = 0.05$, we use the conservative scheme of Eq. (62) to calculate the Lorentz force. The direct simulations of the 3D MHD flows are conducted at $Re = 10$ ($N = 9000$), $Re = 100$ ($N = 900$), $Re = 500$ ($N = 180$) and $Re = 1000$ ($N = 90$). The calculated pressure gradient is compared with Hunt's exact solution. Table 1 listed the calculated and analytical pressure gradient. The relative error in this table is calculated based on the formula of $\text{Error} = \left| \frac{(\nabla p)_{\text{Anal}} - (\nabla p)_{\text{Calc}}}{(\nabla p)_{\text{Anal}}} \right|$. The calculated pressure gradients matches well with the analytical solution when the interaction parameters changed from 9000 to 90.

5.2. Fully 3D simulation – comparing with an experiment for circular pipe

In the fusion blanket, 3-D effects are virtually unavoidable and the flow profiles have a strong influence on heat transfer and corrosion rates. It is essential to validate the fully three-dimensional prediction of the

Table 1
Computed pressure gradient at $Ha = 300$ and $c_w = 0.05$

Reynolds number	10	100	500	1000
Interaction parameter	9000	900	180	90
Calc. ∇p	-374.597	-37.462	-7.491	-3.752
Anal. ∇p	-374.897	-37.490	-7.498	-3.749
Calc. error	0.080%	0.075%	0.093%	0.080%

developed algorithm for a fully 3D MHD flow. While no exact analytical solution exists for 3D MHD flows of interest, experimental data from [37,38] with an axial distribution of the magnetic field varying with either rapid or slow spatial variations is used to compare with the computational results from the consistent and conservative scheme for MHD flows. Fig. 10(a) is a schematic figure of the geometry, and Fig. 10(b) is a comparison of the normalized axial field distributions used for each of the round and rectangular ducts. The coordinate X is an axial distance from the edge of the magnet pole face, non-dimensionalized by the duct half-width.

In [37], two sets of experimental data are reported on the MHD flows in a circular pipe. We simulate the case with a higher Hartmann number and a higher interaction number MHD flow. The detailed parameters corresponding to this case are listed here. The radius is $a = 0.0541$ m. The working fluid has density $\rho = 865$ kg/m³, electrical conductivity $\sigma = 2.86106/(m)$, viscosity $\eta = 8.2175 \times 10^{-4}$ kg/(m s). The thickness of the wall is $t_w = 3.01 \times 10^{-3}$ m, and the conductivity of the wall is $\sigma_w = 1.39 \times 10^6/(m)$. The conductance is $c_w = 0.027$. The applied magnetic field is shown in Fig. 10(b) with the maximum value $B_{max} = 2.08$ T. The inlet average velocity is $U = 0.07$ m/s. The non-dimensional parameters can be calculated as: $Ha = 6640$, $N = 11061$, $Re = 3986$.

We conduct the calculations on a skewed unstructured hexahedral mesh with a fine grid arrangement near the wall. The flow is regarded as a laminar flow, and no turbulence model is employed in the calculation. The velocity on a cell face is interpolated by central averaging the velocities of neighbor cells, which is used to discretize the convective term. No upwind-biased scheme is used to conduct the discretization of the convective term. The discretization of the convective term and the diffusion term has second-order spatial accuracy. The calculated results and experimental results are shown in Figs. 11–14. The solid curves in Figs. 11–13 are the results of the 3-D simulations. This 3D simulation is done using the parallel code of HIMAG [39] implemented with the consistent and conservative scheme developed in this paper for the calculation of the current density and the Lorentz force.

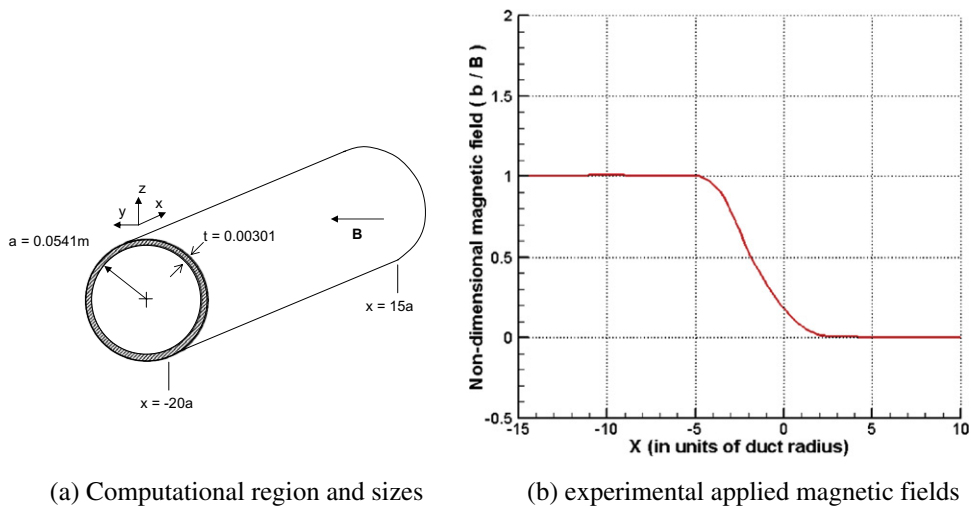


Fig. 10. Computation for $Ha = 6640$ in a circular pipe.

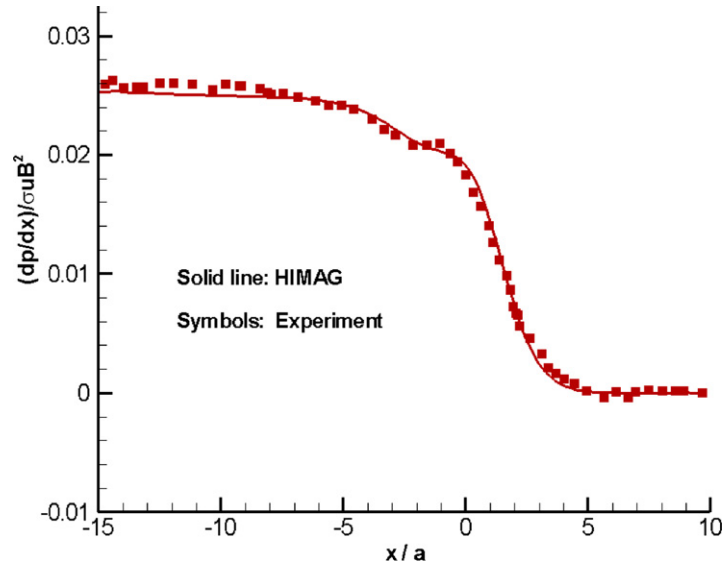


Fig. 11. Pressure gradient comparison along a side layer and a Hartmann layer.

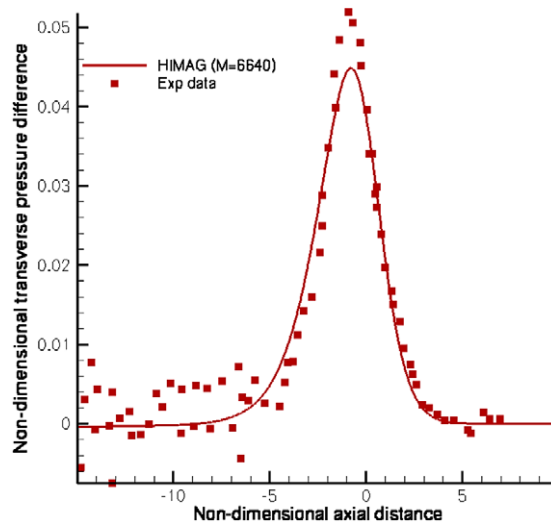


Fig. 12. Transverse pressure difference comparison of computation with measurement.

Fig. 11 presents the axial pressure gradient distribution in a side layer. The pressure gradient in the Hartmann layer is higher than it in the side layer in the fringing region. Fig. 12 presents the transverse pressure difference distributions for roughly the same conditions covered in Fig. 11. The transverse pressure difference is the pressure difference at the wall between the top and the side of the pipe (12 and 3 o'clock) measured at the same axial cross section. In an ordinary fluid flow without a magnetic field, or in a fully developed flow inside a uniform field, the transverse pressure difference is zero. The two behaviors can be asymptotical observed in Fig. 11 at large absolute values of X . The agreement between the experimental data and the 3-D code predictions is very good. The computed maximum pressure difference is slightly smaller than it from the experimental data, which shows that the computed axial pressure gradient in the Hartmann layer is smaller than it from the experiment. Fig. 13 shows the 3D velocity profiles at different positions along the axial direction, which illustrates the processing of the MHD flow from inlet developing flow to outlet fully developed flows. From this velocity profile, we can see that the velocity near the wall is much higher than the velocity at the center.

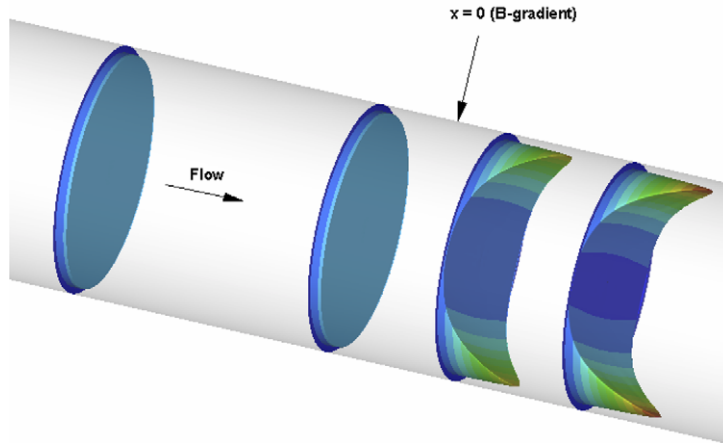


Fig. 13. Velocity profiles along the channel.

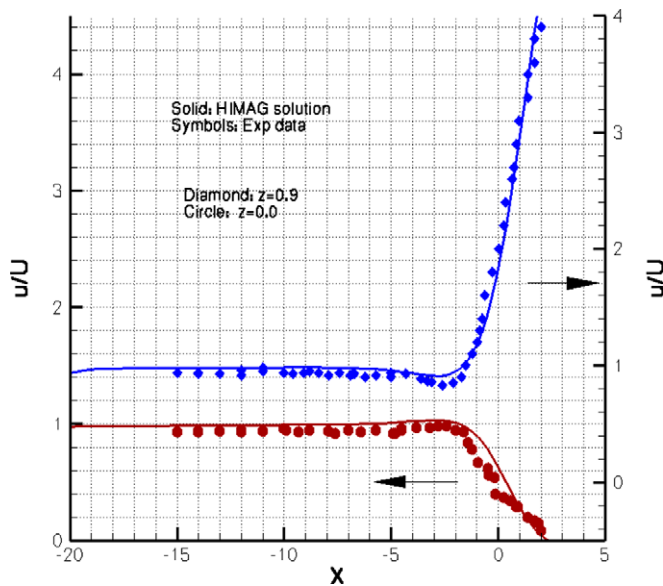


Fig. 14. Velocity profiles comparison against measurement.

Fig. 14 presents two axial velocity distributions from the numerical simulations compared with the experimental data. The lower data in the figure were taken at the duct centerline $z = 0$ ($z = 1.0$ at the duct wall). The upper data were taken at $z = 0.9$. The agreement between the experimental data and the simulation results is excellent. This figure shows dramatically the low velocity core region near the inlet to the magnet, the fringing field area (lower data set) and the high velocity jet region near the walls (upper data set).

Fully three-dimensional computational results were presented and compared to the experimental results from [37,38] of a circular duct geometry on an unstructured mesh. Overall agreement between data and analysis is judged excellent.

6. Conclusion

A conservative formulation in divergence form of the Lorentz force is given in the Navier–Stokes equation. Based on this conservative formula of the Lorentz force, a consistent and conservative scheme has been

designed to simulate MHD flows by solving the electrical potential equations at low magnetic Reynolds numbers on an arbitrary collocated unstructured mesh. The consistent scheme can ensure the calculated current density fluxes on the cell faces of a control volume are divergence-free. The conservative current density fluxes are used to accurately calculate the Lorentz force based on the conservative formulation without any interpolation of the current density from the fluxes on the cell faces to the cell center. Also a conservative interpolation scheme is given to obtain the current density at a cell center from the current fluxes on cell faces. The Lorentz force can also be accurately calculated from the conservative current density at cell centers.

The Lorentz force from the conservative formulation and/or from the conservative current density is conservative, which can ensure the total momentum contributed from the Lorentz force is conservative when the applied magnetic field is spatially independent. The fact that the contribution from the Lorentz force to the total momentum is null for MHD with insulated walls is an important constraint to the scheme design. A scheme, which meets this constraint, can get an accurate result for MHD flows at high Hartmann numbers. The consistent and conservative scheme developed in this paper for an arbitrary collocated unstructured mesh, and in our previous paper [14] for a rectangular collocated mesh meets this constraint, and can be applied for the simulation of MHD flows at low magnetic Reynolds numbers with good accuracy.

Acknowledgments

The authors acknowledge the support from the US Department of Energy. The simulations are conducted using HIMAG [39], in which the consistent projection method and the consistent and conservative schemes are implemented. Leo Bühler is acknowledged for tips on the proper interpretation of experimental data from [37].

Appendix A

In Hunt’s case II of his paper [7], side walls with lengths $2a$ are non-conducting, and Hartmann walls with lengths $2b$ have arbitrary conductivity with $d_B = (t_w \sigma_w)/(a\sigma)$. σ_w is the conductivity of the wall, σ is the conductivity of the liquid and t_w is its thickness. Let $l = b/a$ and suppose that a magnetic field is applied in the y -direction; Hunt [7] gave the analytical solution as a Fourier series in $\xi = x/a \in [-l, l]$, with coefficient functions of $\eta = y/a \in [-l, l]$

$$V = \sum_{k=0}^{\infty} \frac{2(-1)^k \cos(\alpha_k \xi)}{l\alpha_k^3} (1 - V2 - V3) \tag{67}$$

$$V2 = \frac{(1 + \tanh(r_{2k})/(d_B r_{2k})) \cosh(r_{1k} \eta)}{\cosh(r_{1k} \eta)N/r_{2k} + \sinh(r_{1k} + r_{2k})/(d_B r_{2k} \cosh(r_{2k}))} \tag{68}$$

$$V3 = \frac{(1 + \tanh(r_{1k})/(d_B r_{1k})) \cosh(r_{2k} \eta)}{\cosh(r_{2k} \eta)N/r_{1k} + \sinh(r_{1k} + r_{2k})/(d_B r_{1k} \cosh(r_{1k}))} \tag{69}$$

$$H = \sum_{k=0}^{\infty} \frac{2(-1)^k \cos(\alpha_k \xi)}{l\alpha_k^3} (H2 - H3) \tag{70}$$

$$H2 = \frac{(1 + \tanh(r_{2k})/(d_B r_{2k})) \sinh(r_{1k} \eta)}{\cosh(r_{1k} \eta)N/r_{2k} + \sinh(r_{1k} + r_{2k})/(d_B r_{2k} \cosh(r_{2k}))} \tag{71}$$

$$H3 = \frac{(1 + \tanh(r_{1k})/(d_B r_{1k})) \sinh(r_{2k} \eta)}{\cosh(r_{2k} \eta)N/r_{1k} + \sinh(r_{1k} + r_{2k})/(d_B r_{1k} \cosh(r_{1k}))} \tag{72}$$

In Hunt’s formula above

$$N = (Ha^2 + 4\alpha_k^2)^{\frac{1}{2}} \tag{73}$$

$$r_{1k}, r_{2k} = \frac{1}{2} (\pm Ha + (Ha^2 + 4\alpha_k^2)) \tag{74}$$

$$\alpha_k = \left(k + \frac{1}{2}\right) \frac{\pi}{l} \tag{75}$$

Hunt’s formula cannot be directly applied for the calculation using computer code at high Hartmann numbers, since the value of hyperbolic function is out of the range of any existing computer. Considering both r_{1k} and r_{2k} are greater than 0, we reformulate Hunt’s formula as

$$V2 = \frac{\left(d_B r_{2k} + \frac{1 - \exp(-2r_{2k})}{1 + \exp(-2r_{2k})}\right) \frac{\exp(-r_{1k}(1-\eta)) + \exp(-r_{1k}(1+\eta))}{2}}{\frac{1 + \exp(-2r_{1k})}{2} d_B N + \frac{1 + \exp(-2(r_{1k} + r_{2k}))}{1 + \exp(-2r_{2k})}} \tag{76}$$

$$V3 = \frac{\left(d_B r_{1k} + \frac{1 - \exp(-2r_{1k})}{1 + \exp(-2r_{1k})}\right) \frac{\exp(-r_{2k}(1-\eta)) + \exp(-r_{2k}(1+\eta))}{2}}{\frac{1 + \exp(-2r_{2k})}{2} d_B N + \frac{1 + \exp(-2(r_{1k} + r_{2k}))}{1 + \exp(-2r_{1k})}} \tag{77}$$

$$H2 = \frac{\left(d_B r_{2k} + \frac{1 - \exp(-2r_{2k})}{1 + \exp(-2r_{2k})}\right) \frac{\exp(-r_{1k}(1-\eta)) - \exp(-r_{1k}(1+\eta))}{2}}{\frac{1 + \exp(-2r_{1k})}{2} d_B N + \frac{1 + \exp(-2(r_{1k} + r_{2k}))}{1 + \exp(-2r_{2k})}} \tag{78}$$

$$H3 = \frac{\left(d_B r_{1k} + \frac{1 - \exp(-2r_{1k})}{1 + \exp(-2r_{1k})}\right) \frac{\exp(-r_{2k}(1-\eta)) - \exp(-r_{2k}(1+\eta))}{2}}{\frac{1 + \exp(-2r_{2k})}{2} d_B N + \frac{1 + \exp(-2(r_{1k} + r_{2k}))}{1 + \exp(-2r_{1k})}} \tag{79}$$

In a computer code, $\exp(-x)$ can be directly calculated using an intrinsic function in Fortran language, no matter how big a positive value x is. Therefore the above reformulated analytical solution of Eqs. (67), (70), (76)–(79) can be directly applied for the calculation of Hunt’s case II at any Hartmann number. With $d_B = 0$ in the above equations, the reformulated Hunt’s formula can also be used to analyze Shercliff’s case. The calculated V can therefore be used to get the velocity distribution of a fully developed MHD flow, with detailed formula given in [7] as

$$V_z = \mu^{-1} V \left(-\frac{\partial p}{\partial z}\right) a^2 \tag{80}$$

Here μ is the viscosity of liquid. The calculated H can therefore be used to get the current density distribution through the following formula:

$$j_x = \frac{\partial H_z}{\partial y}, \quad j_y = -\frac{\partial H_z}{\partial x} \tag{81}$$

$$H_z = \mu^{-\frac{1}{2}} H \left(-\frac{\partial p}{\partial z}\right) a^2 \sigma^{\frac{1}{2}} \tag{82}$$

For Shercliff’s case, the mean velocity is

$$V_0 = -\frac{2a^2}{l^2 \eta} \frac{dp}{dz} \sum_{k=0}^{\infty} \frac{1}{\alpha_k^4} V_3 \quad \text{with } V_3 = 1 - \frac{N(\cosh(N) - \cosh(Ha))}{2\alpha_k^2 \sinh(N)} \tag{83}$$

V_3 can be reformulated as

$$V_3 = 1 - \frac{N}{2\alpha_k^2} \left(\frac{1 + \exp(-2N)}{1 - \exp(-2N)} - \exp(Ha - N) \frac{1 + \exp(-2Ha)}{1 - \exp(-2N)}\right) \tag{84}$$

which can be directly applied for the computation using a computer code without limitation on the Hartmann numbers.

References

[1] M.A. Abdou et al., On the exploration of innovative concepts for fusion chamber technology fusion, *Fusion Engineering and Design* 54 (2001) 181–247.
 [2] N.B. Morley, S. Smolentsev, R. Munipalli, M.-J. Ni, D. Gao, M.A. Abdou, Progress on the modeling of liquid metal, free surface, MHD flows for fusion liquid walls, *Fusion Engineering Design* 72 (2004) 3–34.

- [3] M. Abdou, D. Sze, C. Wong, M. Sawan, A. Ying, N.B. Morley, S. Malang, US plans and strategy for ITER blanket testing, *Fusion Science and Technology* 47 (2005) 475–487.
- [4] L. Bühler, The influence of small cracks in insulating coatings on MHD and heat transfer in rectangular ducts, *Fusion Engineering and Design* 27 (1995) 634–641.
- [5] J.A. Schercliff, The flow of conducting fluids in circular pipes under transverse magnetic fields, *Journal of Fluid Mechanics* 1 (1956) 644.
- [6] J.A. Schercliff, Steady motion of conducting fluids in pipes under transverse magnetic fields, *Proceedings of Cambridge Philosophical Society* 49 (1953) 126–144.
- [7] J.C.R. Hunt, Magnetohydrodynamic flow in rectangular ducts, *Journal of Fluid Mechanics* 21 (1965) 577–590.
- [8] J.S. Walker, Magnetohydrodynamic flow in rectangular ducts with thin conducting walls, *Journal of Mechanics* 20 (1981) 79.
- [9] A.G. Kulikovskii, Slow steady flows of a conducting fluid at large Hartmann numbers, *Fluid Dynamics* 3 (1968) 1–5.
- [10] L. Bühler, Magnetohydrodynamic flows in arbitrary geometries in strong, nonuniform magnetic fields – a numerical code for the design of fusion reactor blankets, *Fusion Technology* 27 (1994) 3–24.
- [11] S. Molokov, L. Bühler, Liquid metal flow in a U-bend in a strong uniform magnetic field, *Journal of Fluid Mechanics* 267 (1994) 325–352.
- [12] R.J. Moreau, *Magnetohydrodynamics*, Kluwer Academic Publishers, 1990.
- [13] U. Müller, L. Bühler, *Magnetofluidynamics in Channels and Containers*, Springer, 2001.
- [14] M.-J. Ni, R. Munipalli, N.B. Morley, P.Y. Huang, M. Abdou, A Current density conservative scheme for MHD flows at a low magnetic Reynolds number. Part I. On a rectangular collocated grid system, *Journal of Computational Physics*, in press, doi:10.1016/j.jcp.2007.07.025.
- [15] A. Sterl, Numerical simulation of liquid-metal MHD flows in rectangular ducts, *Journal of Fluid Mechanics* 216 (1990) 161–191.
- [16] L. Leboucher, Monotone scheme and boundary conditions for finite volume simulation of magnetohydrodynamic internal flows at high Hartmann number, *Journal of Computational Physics* 150 (1999) 181–198.
- [17] Y. Shimomura, Large eddy simulation of magnetohydrodynamics turbulent channel flows under a uniform magnetic field, *Physics of Fluids A* 3 (1991) 3098.
- [18] N. Umeda, M. Takahashi, Numerical analysis for heat transfer enhancement of a lithium flow under a transverse magnetic field, *Fusion Engineering and Design* (2000) 899–907.
- [19] S. Aleksandrova, S. Molokov, C.B. Reed, Modeling of liquid duct and free-surface flows using CFX, ANL/TD/TM02-30, 2003.
- [20] C. Mistrangelo, Three-dimensional MHD flow in sudden expansion, Ph.D. thesis, der Fakultät für Maschinenbau, der Universität Karlsruhe, 2005.
- [21] W. Kley, On the treatment of the Coriolis force in computational astrophysics, *Journal of Astronomy and Astrophysics* 338 (1998) L37–L41.
- [22] R.K. Agarwal, J.E. Deese, Euler calculations for flow field of a helicopter rotor in Hover, in: *Proceedings of the AIAA 4th Applied Aerodynamics Conference*, San Diego, CA, 1986.
- [23] M. Beddhu, L.K. Taylor, D.L. Whitfield, Strong conservative form of the incompressible Navier–Stokes equations in a rotating frame with a solution procedure, *Journal of Computational Physics* 128 (1996) 427–437.
- [24] ANSYS CFX Home, <http://www-waterloo.ansys.com/>.
- [25] FLUENT Inc., <http://www.fluent.com>.
- [26] Software CRADLE Co., Ltd, <http://www.cradle.co.jp/eindex.htm>.
- [27] P.J. Zwart, The integrated space-time finite volume method, Ph.D. thesis, University of Waterloo, Waterloo, Ontario, Canada, 2000.
- [28] M.-J. Ni, W.-Q. Tao, S.-J. Wang, Stability analysis for discretized steady convective-diffusion equation, *Numerical Heat Transfer, Part B* 35 (1999) 369–388.
- [29] H. Jasak, Error analysis and estimation for the finite volume method with applications to fluid flows, Ph.D. thesis, Imperial College, UK, June 1996.
- [30] M.-J. Ni, M. Abdou, A bridge between projection methods and SIMPLE type methods for incompressible Navier–Stokes equations, *International Journal for Numerical Methods in Engineering*, in press, doi:10.1002/nme.2054.
- [31] J.B. Bell, P. Colella, H.M. Glaz, A second-order projection method for the incompressible Navier–Stokes equations, *Journal of Computational Physics* 85 (1989) 257.
- [32] H. Choi, P. Moin, Effects of the computational time step on numerical solutions of turbulent flow, *Journal of Computational Physics* 113 (1994) 1–4.
- [33] S.V. Patankar, D.B. Spalding, A calculation procedure for heat, mass and momentum transfer in three-dimensional parabolic flows, *International Journal Heat and Mass Transfer* 15 (1972) 1787–1806.
- [34] J.P. Van Doormaal, G.D. Raithby, Enhancement of the SIMPLE method for predicting incompressible fluid flows, *Numerical Heat Transfer* 7 (1984) 147–163.
- [35] M.-J. Ni, M. Abdou, Temporal second-order accuracy of SIMPLE-type methods for incompressible unsteady flows, *Numerical Heat Transfer, Part B* 46 (2005) 529–548.
- [36] Y. Zang, R.L. Street, J.R. Koseff, A non-staggered grid, fractional step method for time-dependent incompressible Navier–Stokes equations in curvilinear coordinates, *Journal of Computational Physics* 114 (1994) 18–33.
- [37] C.B. Reed, Picologlou, T.Q. Hua, J.S. Walker, ALEX results – a comparison of measurements from a round and a rectangular duct with 3-D code predictions, in: *12th Symposium on Fusion Engineering*, Monkey, CA, October 1987.
- [38] T.Q. Hua, B.F. Picologlou, C.B. Reed, J.S. Walker, MHD thermal hydraulic analysis of three-dimensional liquid-metal flows in fusion blanket ducts, *Fusion Engineering and Design* 8 (1989) 241–248.
- [39] R. Munipalli, S. Shankar, M.-J. Ni, N. Morley, Development of a 3-D incompressible free surface MHD computational environment for arbitrary geometries: HIMAG, DOE SBIR phase-ii final report, 2003.